

Optimization of Structural Flood Mitigation Strategies

Byron Tasseff^{1,2}, Russell Bent³, and Pascal Van Hentenryck⁴

¹Department of Industrial and Operations Engineering, University of Michigan, Ann Arbor, Michigan,
USA.

²Information Systems and Modeling Group, Los Alamos National Laboratory, Los Alamos, New Mexico,
USA.

³Applied Mathematics and Plasma Physics Group, Los Alamos National Laboratory, Los Alamos, New
Mexico, USA.

⁴H. Milton Stewart School of Industrial and Systems Engineering, Georgia Institute of Technology,
Atlanta, Georgia, USA.

Key Points:

- Introduction of the structural optimal flood mitigation problem
- Development of problem discretization amenable to derivative-free optimization
- Benefits of constraining the problem with additional physics-based restrictions

This is the author manuscript accepted for publication and has undergone full peer review but has not been through the copyediting, typesetting, pagination and proofreading process, which may lead to differences between this version and the [Version of Record](#). Please cite this article as doi: [10.1029/2018WR024362](https://doi.org/10.1029/2018WR024362)

Corresponding author: Byron Tasseff, btasseff@lanl.gov

Abstract

The dynamics of flooding are primarily influenced by the shape, height, and roughness (friction) of the underlying topography. For this reason, mechanisms to mitigate floods frequently employ structural measures that either modify topographic elevation, e.g., through the placement of levees and sandbags, or increase roughness, e.g., through revegetation projects. However, the configuration of these measures is typically decided in an ad hoc manner, limiting their overall effectiveness. The advent of high-performance surface water modeling software and improvements in black-box optimization suggest that a more principled design methodology may be possible. This paper proposes a new computational approach to the problem of designing structural mitigation strategies under physical and budgetary constraints. It presents the development of a problem discretization amenable to simulation-based, derivative-free optimization. However, meta-heuristics alone are found to be insufficient for obtaining quality solutions in a reasonable amount of time. As a result, this paper proposes novel numerical and physics-based procedures to improve convergence to a high-quality mitigation. The efficiency of the approach is demonstrated on hypothetical dam break scenarios of varying complexity under various mitigation budget constraints. In particular, experimental results show that, on average, the final proposed algorithm results in a 65% improvement in solution quality compared to a direct implementation.

1 Introduction

Modern flood risk management (FRM) is a continuous process of identifying issues, defining objectives, assessing risks, appraising options, implementation, monitoring, and review. Within this framework, risk assessment is regarded as a cyclic process that includes the design and evaluation of alternative management strategies. Such strategies commonly include both “hard” and “soft” structural mitigation measures, e.g., the construction of dams (hard) and wetland storage (soft) (Sayers et al., 2013). Measures can also be temporary (e.g., sandbags) or permanent (e.g., levees). However, for complex scenarios, the number of feasible strategies is extremely large and computationally difficult to explore. As such, the manual design and assessment of these strategies, whether conducted in a real-world or simulation-based setting, can be time-consuming and expensive. This limitation may result in vastly suboptimal FRM strategies. To aid in the FRM

46 process, an optimization-based decision support approach for proposing structural mit-
47 igation designs can serve as a useful tool within the overall risk assessment phase.

48 This paper develops such an optimization-based decision support approach for propos-
49 ing flood protection strategies, whereby effective mitigation designs are realized through
50 the exploration of various configurations in a computational setting. Specifically, the pa-
51 per defines the Optimal Flood Mitigation Problem (OFMP), whose goal is to make to-
52 pographic modifications that protect critical regions under a given flood scenario. This
53 is a difficult optimization problem, as these modifications can have highly nonlinear ef-
54 fects on the flooding behavior. Moreover, physical models used to examine these effects
55 are computationally expensive. Finally, as the OFMP aims at deciding several simulta-
56 neous modifications, an efficient exploration of the full search space is computationally
57 intractable for realistic scenarios.

58 The literature associated with the OFMP is limited. The closest related studies are
59 by D. Judi, Tasseff, Bent, and Pan (2014) and Tasseff, Bent, and Van Hentenryck (2016).
60 In the former, an interdiction model for flood mitigation is proposed, and model surro-
61 gates constructed from simulation data are used as proxies for estimating flood sensi-
62 tivity to hard structural mitigation measures. In the latter, an OFMP similar to that
63 discussed herein is introduced, and mixed-integer linear programs constrained by approx-
64 imate flooding dynamics are solved to obtain hard structural mitigation designs. How-
65 ever, the approach is shown to suffer from substantial scalability issues in space and time.
66 Neither study uses an approach which relies upon repeated deterministic modeling of the
67 partial differential equations (PDEs) underlying the flooding dynamics.

68 A number of studies discuss simulation-optimization approaches for reservoir op-
69 eration, where the PDEs associated with the flood dynamics are treated as a black box.
70 An extensive literature review of these studies can be found in Che and Mays (2015).
71 The work described by Colombo, Guerra, Herty, and Schleper (2009) considers the full
72 PDEs, but their focus is on optimizing normal operations of an open-channel system.
73 Finally, the problem of optimizing dike heights with uncertainty in flooding estimates
74 is considered by Brekelmans, den Hertog, Roos, and Eijgenraam (2012). However, in this
75 study, the PDEs for flood propagation are not considered, and probability models for
76 maximum flood depths are used in place of deterministic physical models.

This paper presents a new approach to the problem of designing structural FRM strategies over PDE constraints. It develops a problem discretization amenable to simulation-based derivative-free optimization. Moreover, the paper shows that meta-heuristics alone are insufficient for obtaining quality solutions in reasonable time. As a result, it presents several innovative computational and physics-based techniques to increase convergence to high-quality solutions. The efficiency of the proposed approach is compared using hypothetical dam break scenarios of varying complexity under multiple mitigation budgets. Experimental results show that the proposed algorithm results in a 65% improvement in solution quality compared to a direct implementation.

The rest of this paper is organized as follows: Section 2 discusses the background of flood modeling and formalization of the OFMP; Section 3 describes solution methods for a specific OFMP; Section 4 compares these methods using fictional dam break scenarios, with both simplistic (Section 4.3) and realistic (Section 4.4) topographies, and multiple mitigation budgets; and Section 5 concludes the paper.

2 Model

In this paper, it is assumed that flood scenarios are modeled using the two-dimensional (2D) shallow water equations. These PDEs are derived from the Navier-Stokes equations under the assumption that horizontal length scales are much larger than the vertical scale. This is reasonable for large-scale floods, where water depths are much smaller than typical flood wavelengths. Two-dimensional models, in particular, alleviate the fundamental disadvantages of their 1D counterparts by allowing for higher-order representations of the topographic surface. Moreover, 2D models readily make use of widely available topographic elevation data. Finally, with recent advances in high-performance computing, solutions to these PDEs have become numerically tractable for large-scale problems, making them of particular computational interest. With volumetric, bed slope, and bed shear stress source terms, these equations are expressed as

$$\frac{\partial h}{\partial t} + \frac{\partial(hu)}{\partial x} + \frac{\partial(hv)}{\partial y} = R(x, y, t), \quad (1a)$$

$$\frac{\partial(hu)}{\partial t} + \frac{\partial}{\partial x} \left(hu^2 + \frac{1}{2}gh^2 \right) + \frac{\partial(huv)}{\partial y} = -gh \frac{\partial B}{\partial x} - g \frac{n^2}{h^{1/3}} |u|u, \quad (1b)$$

$$\frac{\partial(hv)}{\partial t} + \frac{\partial(huv)}{\partial x} + \frac{\partial}{\partial y} \left(hv^2 + \frac{1}{2}gh^2 \right) = -gh \frac{\partial B}{\partial y} - g \frac{n^2}{h^{1/3}} |v|v, \quad (1c)$$

where h is the water depth, u and v are horizontal velocities, B is the bottom topography (or bathymetry), g is the acceleration due to gravity, n is the Manning's roughness

109 coefficient, and R is a volumetric source term (Chertock, Cui, Kurganov, & Wu, 2015).
 110 Equation (1a) represents mass continuity, while Equations (1b) and (1c) represent con-
 111 servation of momentum over the two horizontal dimensions.

112 These equations can be rewritten in vector form by introducing the definitions

$$\begin{aligned}
 \mathbf{U} &:= (h, hu, hv), \quad \mathbf{F}(\mathbf{U}) := \left(hu, hu^2 + \frac{1}{2}gh^2, huv \right), \\
 \mathbf{G}(\mathbf{U}) &:= \left(hv, huv, hv^2 + \frac{1}{2}gh^2 \right), \quad \mathbf{S}_R(R) := (R(x, y, t), 0, 0), \\
 \mathbf{S}_B(\mathbf{U}, B) &:= \left(0, -gh \frac{\partial B}{\partial x}, -gh \frac{\partial B}{\partial y} \right), \quad \mathbf{S}_n := \left(0, -g \frac{n^2}{h^{1/3}} |u|u, -g \frac{n^2}{h^{1/3}} |v|v \right),
 \end{aligned} \tag{2}$$

114 where \mathbf{U} is the vector of conserved variables; \mathbf{F} and \mathbf{G} are fluxes in the x - and y -directions,
 115 respectively; and \mathbf{S}_R , \mathbf{S}_B , and \mathbf{S}_n are the volumetric, bed slope, and bed shear stress source
 116 terms, respectively. This allows Equations (1a), (1b), and (1c) to be rewritten more con-
 117 cisely as

$$\mathbf{U}_t + \mathbf{F}_x + \mathbf{G}_y = \mathbf{S}_R + \mathbf{S}_B + \mathbf{S}_n, \tag{3}$$

119 where t , x , and y indicate partial differentiation with respect to those variables.

120 The OFMP considers a flood scenario (e.g., a dam failure) and a set of 2D regions
 121 (“assets”) to protect. To minimize flooding at asset locations, the model must produce
 122 optimal topographic elevation and roughness fields using a set of m mitigation measures.
 123 For each measure $i \in \{1, 2, \dots, m\}$, the functions $\delta_B(\omega_i)$ and $\delta_n(\omega_i)$ define 2D fields of
 124 height and roughness for a given tuple of field parameters ω_i . Measures can first addi-
 125 tively modify the elevation field B to return a new field \tilde{B} , defined as

$$\tilde{B}(B, (\omega_1, \omega_2, \dots, \omega_m)) := B + \sum_{i=1}^m \delta_B(\omega_i). \tag{4}$$

127 Similarly, measures can modify the roughness field n to return a new field defined as

$$\tilde{n}(n, (\omega_1, \omega_2, \dots, \omega_m)) := n + \{\max_i \{\delta_n(\omega_i)(x, y)\} : (x, y) \in \mathbb{R}^2\}, \tag{5}$$

129 i.e., a field of maximum roughness. For notational ease, hereafter, \tilde{B} refers to Equation
 130 4, \tilde{n} refers to Equation 5, and the tuple $(\omega_1, \omega_2, \dots, \omega_m)$ is referred to as the “paramet-
 131 ric configuration,” or simply the “configuration.” With these definitions and shorthand
 132 notations, the *modified* bed slope source term is defined as

$$\tilde{\mathbf{S}}_B(\mathbf{U}, B, (\omega_1, \omega_2, \dots, \omega_m)) := \left(0, -gh \frac{\partial \tilde{B}}{\partial x}, -gh \frac{\partial \tilde{B}}{\partial y} \right). \tag{6}$$

134 We note that the change in elevation may be a result of permanent structures such as
 135 levees or temporary measures such as sandbags. Similarly, the modified bed shear stress

136 source term is defined as

$$137 \quad \tilde{\mathbf{S}}_n(\mathbf{U}, n, (\omega_1, \omega_2, \dots, \omega_m)) := \left(0, -g \frac{\tilde{n}^2}{h^{1/3}} |u|u, -g \frac{\tilde{n}^2}{h^{1/3}} |v|v \right). \quad (7)$$

138 Hereafter, $\tilde{\mathbf{S}}_B := \tilde{\mathbf{S}}_B(\mathbf{U}, B, (\omega_1, \omega_2, \dots, \omega_m))$ and $\tilde{\mathbf{S}}_n := \tilde{\mathbf{S}}_n(\mathbf{U}, n, (\omega_1, \omega_2, \dots, \omega_m))$
139 are used to concisely denote these two source terms that vary with the configuration.

140 The OFMP is then written in a form that embeds the 2D shallow water equations
141 as constraints and optimizes the tuple $(\omega_1, \omega_2, \dots, \omega_m)$ (i.e., the configuration) via

$$142 \quad \underset{\omega_1, \omega_2, \dots, \omega_m}{\text{minimize}} \quad z(\omega_1, \omega_2, \dots, \omega_m) = \sum_{a \in \mathcal{A}} \iint_a \max_t h(x, y, t) \, dx \, dy \quad (8a)$$

$$143 \quad \text{subject to} \quad \mathbf{U}_t + \mathbf{F}_x + \mathbf{G}_y = \mathbf{S}_R + \tilde{\mathbf{S}}_B + \tilde{\mathbf{S}}_n \quad (8b)$$

$$144 \quad \delta_B(\omega_i)(x, y) = 0, \quad \forall i \in \{1, 2, \dots, m\}, \quad \text{for } (x, y) \in \bigcup \mathcal{A} \quad (8c)$$

$$145 \quad \delta_n(\omega_i)(x, y) = 0, \quad \forall i \in \{1, 2, \dots, m\}, \quad \text{for } (x, y) \in \bigcup \mathcal{A} \quad (8d)$$

$$146 \quad (\omega_1, \omega_2, \dots, \omega_m) \in \mathcal{F}. \quad (8e)$$

148 Here, \mathcal{A} denotes the set of asset regions to be protected and z denotes the objective func-
149 tion. This function is defined in Equation (8a) and captures the maximum water vol-
150 ume over all asset locations and times. Constraint (8b) denotes the solution to the shal-
151 low water equations in the presence of the m mitigation measures. Constraints (8c) pro-
152 hibit measures from being constructed “underneath” an asset. Similarly, Constraints (8d)
153 prohibit the roughness at an asset location from being modified. Finally, Constraint (8e)
154 ensures $(\omega_1, \omega_2, \dots, \omega_m)$ resides within the set of all feasible parametric configurations
155 \mathcal{F} , i.e., \mathcal{F} distinguishes valid and invalid mitigation designs.

156 For simplicity of presentation, this paper considers only two types of structural mea-
157 sures, although the approach can easily be generalized to include other soft and hard mea-
158 sures, both temporary and permanent. The first type is an immovable wall of fixed length
159 (ℓ) , width (w) , and height (\bar{b}_i) . Each wall is defined using three continuously-defined,
160 bounded parameters: latitudinal position of the wall centroid (λ_i) , longitudinal position
161 of the wall centroid (ϕ_i) , and angle of the wall formed with respect to the longitudinal
162 axis (θ_i) . In this paper, the centroid position is bounded by the scenario domain’s spa-
163 tial extent, and $\theta_i \in [0, \pi]$. The second structural type is a revegetation project defined
164 by a 2D circular region with center (λ_i, ϕ_i) and fixed radius r that increases the area’s
165 Manning’s roughness coefficient based on a fixed field \bar{n}_i . Under these assumptions, the
166 OFMP aims at deciding $\omega_i = (\lambda_i, \phi_i, \theta_i, \bar{b}_i, \bar{n}_i)$ for each measure $i \in \{1, 2, \dots, m\} =$

167 \mathcal{M} , where \bar{b}_i and \bar{n}_i are decided a priori for each measure. More specifically, this pro-
 168 duces an OFMP of the specialized form

$$169 \quad \underset{\omega_1, \omega_2, \dots, \omega_m}{\text{minimize}} \quad z(\omega_1, \omega_2, \dots, \omega_m) = \sum_{a \in \mathcal{A}} \iint_a \max_t h(x, y, t) \, dx \, dy \quad (9a)$$

$$170 \quad \text{subject to} \quad \mathbf{U}_t + \mathbf{F}_x + \mathbf{G}_y = \mathbf{S}_R + \tilde{\mathbf{S}}_B + \tilde{\mathbf{S}}_n \quad (9b)$$

$$171 \quad \delta_B(\omega_i)(x, y) = 0, \text{ for } (x, y) \in \bigcup \mathcal{A}, \forall i \in \mathcal{M} \quad (9c)$$

$$172 \quad \delta_n(\omega_i)(x, y) = 0, \text{ for } (x, y) \in \bigcup \mathcal{A}, \forall i \in \mathcal{M} \quad (9d)$$

$$173 \quad \delta_B(\omega_i)(x, y) = \begin{cases} \bar{b}_i & \text{for } \begin{cases} |(x - \phi_i) \cos \theta_i - (y - \lambda_i) \sin \theta_i| \leq \frac{\ell}{2} \\ |(x - \phi_i) \sin \theta_i + (y - \lambda_i) \cos \theta_i| \leq \frac{w}{2} \end{cases} \\ 0 & \text{otherwise} \end{cases} \forall i \in \mathcal{M} \quad (9e)$$

$$174 \quad \delta_n(\omega_i)(x, y) = \begin{cases} \bar{n}_i(x, y) & \text{for } (x - \phi_i)^2 + (y - \lambda_i)^2 \leq r^2 \\ 0 & \text{otherwise} \end{cases} \forall i \in \mathcal{M} \quad (9f)$$

$$175 \quad \lambda_{lb} \leq \lambda_i \leq \lambda_{ub}, \phi_{lb} \leq \phi_i \leq \phi_{ub}, 0 \leq \theta_i \leq \pi, \forall i \in \mathcal{M}. \quad (9g)$$

177 Using this formulation, i is a wall when $\bar{b}_i > 0$ and $\bar{n}_i = 0$, and i is a revegetation project
 178 when $\bar{b}_i = 0$ and $\bar{n}_i > 0$. Constraints (9c) and (9d) emphasize that modifications can-
 179 not be made within asset regions; Constraints (9e) impose the wall height \bar{b}_i within each
 180 rotated rectangle defined using the parameters λ_i , ϕ_i , and θ_i and a standard 2D rota-
 181 tion matrix; and Constraints (9f) impose additions to roughness within each revegeta-
 182 tion circle defined by the center (λ_i, ϕ_i) . Finally, Constraints (9g) replace Constraint (8e)
 183 of the more general OFMP. Here, λ_{lb} and λ_{ub} (ϕ_{lb} and ϕ_{ub}) are the lower and upper lat-
 184 itudinal (longitudinal) boundaries of the scenario domain.

185 Constraints (9g) imply a large feasible region, as the spatial extent is typically much
 186 larger than the flood's extent. To reduce the solution space, the notion of a *restricted*
 187 *region* \mathcal{P} is thus introduced, where centroids must reside in \mathcal{P} . That is,

$$188 \quad (\lambda_i, \phi_i) \in \mathcal{P}, \forall i \in \{1, 2, \dots, m\} \quad (9h)$$

189 is appended to the problem above, completing the primary model used in this paper.

190 3 Algorithm

191 The OFMP at the end of Section 2 remains difficult to solve directly. However, with
 192 recent improvements in both numerical discretizations of the shallow water equations (e.g.,
 193 Chertock et al. (2015)) and high-performance implementations thereof (e.g., Brodtkorb,

194 Sætra, and Altinakar (2012), Tasseff (2016)), numerically efficient solutions of the PDEs
 195 described in Constraint (9b) are possible. With this intuition, in Algorithm 1, a time-
 196 limited search-based method is introduced to find a near-optimal solution $(\omega_1^*, \omega_2^*, \dots, \omega_m^*)$
 197 to the problem defined by Equations (9a) through (9h).

Algorithm 1 SOLVEOFMP: Solves the OFMP defined by Equations (9a) through (9h).

```

1: function SOLVEOFMP( $B, n, \mathcal{A}, m, T_{\max}, \alpha$ )
2:    $\tilde{\mathcal{P}} \leftarrow \text{INITIALIZERESTRICTION}(B, n, \mathcal{A}, \alpha)$ 
3:    $(\omega_1^*, \omega_2^*, \dots, \omega_m^*) \leftarrow \text{INITIALIZESOLUTION}(m, \tilde{\mathcal{P}}), \Omega \leftarrow \emptyset$ 
4:   while CLOCK  $< T_{\max}$  do
5:      $(\omega_1, \omega_2, \dots, \omega_m) \leftarrow \text{GENERATESOLUTION}(m, \tilde{\mathcal{P}}, \Omega)$ 
6:     Solve  $\mathbf{U}_t + \mathbf{F}_x + \mathbf{G}_y = \mathbf{S}_R + \tilde{\mathbf{S}}_B + \tilde{\mathbf{S}}_n$ 
7:      $\Omega \leftarrow \Omega \cup \{(\omega_1, \omega_2, \dots, \omega_m)\}$ 
8:     if  $z(\omega_1, \omega_2, \dots, \omega_m) < z(\omega_1^*, \omega_2^*, \dots, \omega_m^*)$  then
9:        $(\omega_1^*, \omega_2^*, \dots, \omega_m^*) \leftarrow (\omega_1, \omega_2, \dots, \omega_m)$ 
10:       $\tilde{\mathcal{P}} \leftarrow \text{UPDATERESTRICTION}(\mathbf{U}, \mathcal{A}, \tilde{\mathcal{P}}, \alpha)$ 
11:    end if
12:  end while
13:  return  $(B + \sum_{i=1}^m \delta_B(\omega_i^*), n + \{\max_i \{\delta_n(\omega_i^*)(x, y)\} : (x, y) \in \mathbb{R}^2\})$ 
14: end function

```

198 Here, B and n denote the initial topographic elevation and Manning's roughness
 199 coefficient fields; \mathcal{A} denotes the set of assets; m denotes the number of mitigation mea-
 200 sures being configured; T_{\max} denotes the maximum clock time; and α is a parameter used
 201 for computing restrictions. The function CLOCK returns the current clock time. Since
 202 a useful definition of \mathcal{P} is difficult to compute a priori, $\tilde{\mathcal{P}}$ serves as an iterative approx-
 203 imation of some desired \mathcal{P} . In Line 2, $\tilde{\mathcal{P}}$ is initialized; it is later modified in Line 10 us-
 204 ing UPDATERESTRICTION. Both functions are described in Section 3.1. In Line 3, the
 205 best solution and the historical solution set Ω are initialized. In Line 5, a configuration
 206 is generated via some history-dependent function GENERATESOLUTION, described in Sec-
 207 tion 4.1. In Line 6, the shallow water equations are solved. In Line 7, the historical so-
 208 lution set is updated. In Lines 8 through 11, the best solution and $\tilde{\mathcal{P}}$ are updated. Fi-
 209 nally, in Line 13, the best elevation and roughness fields are returned.

3.1 Computation of the restricted region

3.1.1 The direct methodology

The most obvious globally acceptable method for selecting \mathcal{P} is to assume

$$\mathcal{P} = \mathbb{R}^2, \quad (10)$$

where, of course,

$$\{(x, y) \in \mathbb{R}^2 : \lambda_{lb} \leq x \leq \lambda_{ub}, \phi_{lb} \leq y \leq \phi_{ub}\} \subset \mathcal{P}, \quad (11)$$

indicating the bounds within Constraints 9g involving λ_i and ϕ_i dominate those imposed by \mathcal{P} . This method for selecting \mathcal{P} is hereafter referred to as the direct method. In practice, this method is used to define the direct implementations of the functions INITIALRESTRICTION and UPDATERESTRICTION, both of which return the set \mathbb{R}^2 .

3.1.2 The pathline methodology

A *pathline* is the trajectory an individual fluid element follows over time, beginning at position (x_0, y_0) and time t_0 . In 2D, a pathline is defined by the two equations

$$x(t) = x_0 + \int_{t_0}^t u(x(t'), y(t'), t') dt', \quad (12a)$$

$$y(t) = y_0 + \int_{t_0}^t v(x(t'), y(t'), t') dt', \quad (12b)$$

where u and v are velocities in the x - and y -directions. To compute the pathline from a flood wave to an initially dry point (x_0, y_0) , the definition of $t_{\text{wet}}(x_0, y_0)$ is introduced as the time at which the depth at (x_0, y_0) exceeds some threshold. More concisely,

$$t_{\text{wet}}(x_0, y_0) := \min \{t \in [t_0, t_f] : h(x_0, y_0, t) \geq \epsilon_h\}, \quad (13)$$

where ϵ_h is an arbitrarily small depth, taken in this study to be one millimeter. Using this definition, the pathline equations may be integrated *in reverse*, giving

$$x_{\text{wet}}(x_0, y_0, t) = x_0 + \int_{t_{\text{wet}}}^t u(x_{\text{wet}}(t'), y_{\text{wet}}(t'), t') dt', \quad (14a)$$

$$y_{\text{wet}}(x_0, y_0, t) = y_0 + \int_{t_{\text{wet}}}^t v(x_{\text{wet}}(t'), y_{\text{wet}}(t'), t') dt', \quad (14b)$$

where it is assumed that $t \leq t_{\text{wet}}$. The above equations approximate a path to flooding.

In this paper, a *pathtube* is defined as a set of pathlines satisfying Equations (14a) and (14b). For a region \mathcal{R} , the pathtube \mathcal{S} encompassing \mathcal{R} with a start time of t_0 is

$$\mathcal{S}(\mathbf{U}, \mathcal{R}) = \{(x_{\text{wet}}(x_0, y_0, t), y_{\text{wet}}(x_0, y_0, t)) \in \mathbb{R}^2 : (x_0, y_0) \in \mathcal{R}, t \in [t_0, t_{\text{wet}}(x_0, y_0)]\}. \quad (15)$$

This region encompasses approximate paths of least resistance from a flood to \mathcal{R} . It is clear that good locations for structural mitigation measures are likely to reside in \mathcal{S} .

A robust selection of \mathcal{P} would account for the change in \mathbf{U} with respect to a large set of feasible configurations. In an ideal setting, a good selection for \mathcal{P} would thus be

$$\mathcal{P} = \bigcup_{\omega \in \mathcal{F}} \bigcup_{a \in \mathcal{A}} \{(x, y) \in \mathcal{S}(\mathbf{U}, a) : \mathbf{U}_t + \mathbf{F}_x + \mathbf{G}_y = \mathbf{S}_R + \tilde{\mathbf{S}}_B + \tilde{\mathbf{S}}_n\}. \quad (16)$$

In practice, defining \mathcal{P} as per Equation (16) is nontrivial. First, each $a \in \mathcal{A}$ may be a set of infinitely many points. There are also infinitely many moments t in a solution \mathbf{U} to the shallow water equations. Most importantly, the union over all feasible configurations $(\omega_1, \omega_2, \dots, \omega_m) = \omega \in \mathcal{F}$ assumes knowledge of \mathbf{U} for any such feasible configuration $(\omega_1, \omega_2, \dots, \omega_m)$. For these reasons, an iteratively-constructed definition of the pathtube-like region $\tilde{\mathcal{P}}$ is instead proposed, which approximately captures the features of some unknown larger \mathcal{P} relevant to the OFMP (e.g., Equation (16)).

From a numerical perspective, each $a \in \mathcal{A}$ is actually a polygon whose exterior connects a set of points P_a . Solutions to the OFMP are likely to intersect the pathlines from a flood to each of these points. Also, in practice, numerical solutions to the shallow water equations are discrete in space and time. Assuming that solutions are obtained for a set of timestamps \mathcal{T} on a rectangular grid G , t_{wet} is first redefined as

$$t_{\text{wet}}(x_0, y_0) := \min\{t \in \mathcal{T} : h_{i_0, j_0, t} \geq \epsilon_h\}, \quad (17)$$

where (i_0, j_0) is the unique index of the cell in grid G that contains the point (x_0, y_0) .

For each point along an asset exterior, a numerical representation of the pathline leading to that point is desired. To accomplish this, it is assumed that a pathline can be approximated as a set \mathcal{L} of discrete points. These points can be generated by solving Equations (14a) and (14b) using any suitable ODE integration technique. In this study, suggestions from Telea (2014) (initially described for *streamlines*, which trace a static field) are used to compute pathlines according to the function `COMPUTE_PATHLINE`(\mathbf{U}, x_0, y_0), whose arguments denote a solution \mathbf{U} to the shallow water equations and the x - and y -positions of a seed point, respectively. A complete description of this function is given in the appendix (Algorithm 3).

The definition of COMPUTEPATHLINE enables the computation of a set of points Q approximating the *pathtube* leading to a set of exterior asset points $P_a \in a \in \mathcal{A}$ via

$$Q(\mathbf{U}, P_a) = \bigcup_{(x_0, y_0) \in P_a} \text{COMPUTEPATHLINE}(\mathbf{U}, x_0, y_0). \quad (18)$$

Since pathtubes are curvilinear, typical geometries that envelope Q (e.g., the convex hull) do not effectively summarize this set. For this reason, the notion of an *alpha shape* is introduced, which minimally encompasses points of Q using straight lines. A discussion on alpha shapes can be found in Fischer (2000). In this study, Edelsbrunner's algorithm (Edelsbrunner, Kirkpatrick, and Seidel (1983)), presented in the appendix (Algorithm 4), is used to compute alpha shapes. The function that computes this shape for a set Q and alpha value α is denoted as ALPHASHAPE(Q, α).

The definition of the function ALPHASHAPE finally allows for definition of the functions INITIALIZERESTRICTION and UPDATERESTRICTION. Both assume restrictions are the unions of alpha shapes approximating the pathtubes leading to each asset. The functions are described in Algorithms 2 and Equation (19), respectively. In Algorithm 2, Line 2, the shallow water equations are solved *without* the presence of structural mitigation measures. In Line 3, the union of alpha shapes for all pathtubes leading to the assets $a \in \mathcal{A}$ is computed. Asset regions are then subtracted from this set to ensure structural measures do not overlap with asset locations.

The function UPDATERESTRICTION using the pathline approach is defined as

$$\text{UPDATERESTRICTION}(\mathbf{U}, \mathcal{A}, \mathcal{P}, \alpha) = \mathcal{P} \cup \left(\bigcup_{a \in \mathcal{A}} \text{ALPHASHAPE}(Q(\mathbf{U}, P_a), \alpha) \right) \setminus \bigcup \mathcal{A}. \quad (19)$$

The majority of this function resembles Algorithm 2, although the union of the current set and previous \mathcal{P} is computed to encourage exploration of a more representative (i.e., expanded) search space. Moreover, as per Algorithm 1, this function is only called as better solutions to the OFMP are obtained. This decreases the burden of computing pathtubes and alpha shapes on each iteration of the algorithm.

3.2 Sequential optimization algorithm

Due to the nonlinear sensitivity of flooding behavior with respect to mitigation efforts, predictable and incremental changes to solutions of the OFMP while increasing the number of mitigation measures, m , are not ensured. This may be undesirable from a planning perspective. A separate algorithm is thus proposed to induce a sequential so-

Algorithm 2 INITIALIZERESTRICTION: Returns the initial restricted positional set.

```

1: function INITIALIZERESTRICTION( $B, n, \mathcal{A}, \alpha$ )
2:   Solve  $\mathbf{U}_t + \mathbf{F}_x + \mathbf{G}_y = \mathbf{S}_R + \mathbf{S}_B + \mathbf{S}_n$ 
3:   return  $\bigcup_{a \in \mathcal{A}} \text{ALPHASHAPE}(Q(\mathbf{U}, P_a), \alpha) \setminus \bigcup \mathcal{A}$ 
4: end function

```

298 lution to the OFMP, whereby solutions with $m = 2$ include those of $m = 1$, solutions
 299 with $m = 3$ include those of $m = 2$, and so on. This ensures increasing utility for con-
 300 figurations of increasing sizes. It also allows policymakers to more clearly understand the
 301 effects of budgetary constraints with respect to the overall structural flood mitigation
 302 efforts. The recursion to compute sequential solutions may be defined as

$$303 \quad (B_i, n_i) = \text{SOLVEOFMP} \left(B_{i-1}, n_{i-1}, \mathcal{A}, 1, \frac{T_{\max}}{m}, \alpha \right), \quad (20)$$

304 where $B_0 = B$, $n_0 = n$, and the time for each subproblem is an equal portion of T_{\max} .
 305 In this paper, Line 10 is eliminated from Algorithm 1 when using the sequential approach,
 306 as the best placement for a *single* structural mitigation measure is likely to reside within
 307 the *initial* $\tilde{\mathcal{P}}$ computed on Line 2. As a consequence, for each structural measure placed
 308 using the sequential approach, pathtubes are constructed only once.

309 4 Results

310 4.1 Model relaxation

311 The proposed approach uses the open source `scipy.optimize.differential_evolution`
 312 (DE) and `RBFOpt` libraries to produce two separate implementations of GENERATES-
 313 OLUTION in Algorithm 1 (Costa & Nannicini, 2014; Storn & Price, 1997). Both only in-
 314 clude support for simple bounds like those indicated in Constraints (9g). Thus, these im-
 315 plementations of GENERATESOLUTION may generate configurations that are infeasible
 316 with respect to Constraints (9c) through (9f). To overcome this, the OFMP defined by

317 Equations (9a) through (9h) is replaced with the relaxed formulation

$$318 \quad \underset{\omega_1, \omega_2, \dots, \omega_m}{\text{minimize}} \quad z(\omega_1, \omega_2, \dots, \omega_m) = p_1 + p_2 + \sum_{a \in \mathcal{A}} \iint_a \max_t h(x, y, t) \, dx \, dy \quad (21a)$$

$$319 \quad \text{subject to} \quad p_1 = c_1 \sum_{i=1}^m \min \{ \|(x, y) - (\lambda_i, \phi_i)\| : (x, y) \in \mathcal{P} \} \quad (21b)$$

$$320 \quad p_2 = c_2 \sum_{i=1}^m \sum_{a \in \mathcal{A}} \iint_a \delta_B(\omega_i) \, dx \, dy + c_3 \sum_{i=1}^m \sum_{a \in \mathcal{A}} \iint_a \delta_n(\omega_i) \, dx \, dy \quad (21c)$$

$$321 \quad \mathbf{U}_t + \mathbf{F}_x + \mathbf{G}_y = \mathbf{S}_R + \tilde{\mathbf{S}}_B + \tilde{\mathbf{S}}_n \quad (21d)$$

$$322 \quad \delta_B(\omega_i)(x, y) = \begin{cases} \bar{b}_i & \text{for } \begin{cases} |(x - \phi_i) \cos \theta_i - (y - \lambda_i) \sin \theta_i| \leq \frac{\ell}{2} \\ |(x - \phi_i) \sin \theta_i + (y - \lambda_i) \cos \theta_i| \leq \frac{w}{2} \end{cases} \\ 0 & \text{otherwise} \end{cases} \quad \forall i \in \mathcal{M} \quad (21e)$$

$$323 \quad \delta_n(\omega_i)(x, y) = \begin{cases} \bar{n}_i & \text{for } (x - \phi_i)^2 + (y - \lambda_i)^2 \leq r^2 \\ 0 & \text{otherwise} \end{cases} \quad \forall i \in \mathcal{M} \quad (21f)$$

$$324 \quad \lambda_{lb} \leq \lambda_i \leq \lambda_{ub}, \quad \phi_{lb} \leq \phi_i \leq \phi_{ub}, \quad 0 \leq \theta_i \leq \pi, \quad \forall i \in \mathcal{M}. \quad (21g)$$

326 In Equation (21a), two penalty terms are included in the objective to capture infeasibilities in Constraints (9c) through (9f). The first penalty, p_1 , is defined in Constraint 327 (21b) and denotes the sum of all minimum distances between each measure's centroid 328 and the nearest point of the restricted positional set \mathcal{P} . This term is scaled by the constant 329 c_1 , taken in this study to be equal to one. The second penalty, p_2 , is defined in Constraint 330 (21c). Here, the first term denotes the net modified elevation volume over all asset 331 regions, and the second term denotes the net change in roughness over all asset 332 regions. These terms are scaled by the constants c_2 and c_3 , respectively. Herein, both are 333 taken to be $(\Delta r)^{-2}$, where Δr is the spatial resolution of the discretization. 334

335 4.2 Experimental setting

336 For simplicity, Sections 4.3 through 4.4.3 focus on OFMPs where only wall-type 337 measures are considered (i.e., $\bar{b}_i > 0$), while Section 4.4.4 presents an algorithmic proof 338 of concept where only revegetation-type measures are considered (i.e., $\bar{n}_i > 0$). For each 339 experiment, Algorithm 1 was limited to one day of wall-clock time. When using DE, population 340 sizes of $45m$ ($\bar{b}_i > 0$) and $30m$ ($\bar{n}_i > 0$) were employed; trial solutions were 341 computed as the best solution plus scaled contributions of two random candidates; the 342 mutation constant varied randomly within $[0.5, 1.0]$; and the recombination constant was 343 set to 0.9. When using the direct INITIALIZERRESTRICTION and UPDATERESTRICTION

344 methods, Latin hypercube sampling was used to initialize the population. When using
345 the pathline-based methods, the population was initialized via random sampling over the
346 initial restricted set (i.e., $\tilde{\mathcal{P}}$) and $\theta_i \in [0, \pi]$. When using RBFOpt, the **sampling** method
347 was used; most other parameters were left unchanged.

348 For computational considerations, if the configuration proposed by GENERATES-
349 OLUTION was feasible, the shallow water equations (i.e., Constraint (21d)) were solved
350 using the proposed configuration. Otherwise, a solution containing *no structural miti-*
351 *gation measures* was referenced. That is, \tilde{S}_B was replaced with S_B , and \tilde{S}_n was replaced
352 with S_n . To solve these PDEs, the open-source surface-water modeling software Nuflood
353 (Tasseff, 2016) was used, where the shallow water equations are spatially discretized ac-
354 cording to the scheme described by Kurganov and Petrova (2007).

355 Each experiment was conducted on one Intel Xeon E5-2695 V4 CPU containing
356 eighteen cores at 2.1 GHz and 125 GB of RAM. Nuflood was compiled in single-precision
357 mode using the Intel C++ Compiler, version 17.0.1. The remainder of Algorithm 1 was
358 implemented in Python 3.6. Compared to the PDE evaluations, these other portions of
359 the algorithm were found to be computationally negligible.

360 4.3 Simplified circular dam break scenarios

361 To compare the two positional restriction methodologies described in Section 3.1,
362 six simple OFMP scenarios were constructed. All were intended to have human intuitive
363 solutions, i.e., optimal placement of structural mitigation measures could be inferred from
364 a basic understanding of flood propagation. These scenarios are displayed pictorially in
365 Figure 1. In each scenario, under the influence of gravity, the initial volume of water (col-
366 ored with blue) is propagated outward; without mitigation measures, this water comes
367 into contact with assets (colored with red), flooding them.

368 Each of the six scenarios was modeled using a spatial resolution of one meter and
369 64×64 grid cells. The ground surface was assumed to be frictionless; critical depth bound-
370 ary conditions were employed; and a simulation duration of one hundred seconds was used.
371 When necessary to compute pathlines, intermediate PDE solution data was reported for
372 every one second of simulation time. In the experiments performed, each of the corre-
373 sponding OFMPs was solved with the number of walls, m , ranging from one to five. Wall

374 widths, lengths, and heights were fixed to 2.5, 8.0, and 1.0 meters, respectively. Finally,
375 all experiments were performed using a single fixed random seed.

376 In Figure 2, for each experiment, the objective behavior is plotted against the num-
377 ber of PDE evaluations required to reach that objective. These behaviors are compared
378 for the direct differential evolution solver (DE-D) and its pathline-based counterpart (DE-
379 PL). The DE-PL solver was generally able to find good solutions faster and improve upon
380 them more rapidly, especially for configurations involving larger numbers of walls. How-
381 ever, there were some instances where the DE-D solver produced higher quality solutions
382 than the DE-PL solver, e.g., when optimizing the configuration of five walls in Scenario
383 4. These anomalies could be a consequence of the random nature of the DE algorithm;
384 they could also be due to the DE implementation's tendency to terminate once a pop-
385 ulation has sufficiently stabilized.

386 In Figure 3, the best obtained wall configurations using DE-PL are displayed pic-
387 torially for all pairs of scenarios and numbers of mitigation measures. The configurations
388 resemble what might be intuited by a human. When applicable, configurations are non-
389 overlapping and well-connected. As the number of walls varies, configurations also show
390 interesting nonincremental behavior. For example, in the first scenario, walls are initially
391 placed close to the asset; as the number of walls increases, they are placed farther away
392 to form connections with existing topographic features. However, such non-sequential
393 behavior may be undesirable from a planning perspective.

394 **4.4 Hypothetical dam break scenario from Theme C of the 12th Inter-** 395 **national Benchmark Workshop on Numerical Analysis of Dams**

396 This section focuses on demonstrating the merits of the sequential optimization al-
397 gorithm using the hypothetical dam break defined in Theme C of the 12th International
398 Benchmark Workshop on Numerical Analysis of Dams (ICOLD 2013) (D. R. Judi, Pasqualini,
399 & Arnold, 2014). To simulate this scenario, the dam break was modeled as a point source
400 with time-dependent discharge. The initial topographic elevation field (with the dam ex-
401 cluded) was provided by the workshop and resampled from a resolution of ten to ninety
402 meters to ease computational burden. The Manning's roughness coefficient was set to
403 0.035; critical depth boundary conditions were employed; a duration of twelve hours was

used; and, when necessary to compute pathlines, PDE solution data was reported every ten minutes of simulation time.

Asset locations and sizes were selected to increase the difficulty of the OFMP, with two assets placed near the primary channel of the scenario and three placed farther away. The experimental setup remained similar to that described in Section 4.3. However, in this case, the number of walls ranged from one to ten, while wall widths, lengths, and heights were fixed to 250, 1000, and ten meters, respectively. To compare differences in OFMP solver performance, each solver was executed using ten different random seeds for each possible number of walls. In total, the experiments described in this subsection thus required nearly six hundred days of compute time.

4.4.1 Pathline-based algorithm results

To confirm the effectiveness of the pathline-based solvers, two implementations of Algorithm 1 using RBFOpt were benchmarked. In Table 1, the objective behavior of the pathline-based solver (RBFOpt-PL) is compared against its direct counterpart (RBFOpt-D). The pathline-based solver clearly outperformed RBFOpt-D in nearly all instances, e.g., it resulted in smaller minima, means, and standard deviations. The single exception appears to be for $m = 1$, where the direct solver produced an equivalent minimum to the pathline-based solver. Nonetheless, on average, the pathline-based solver provided a 45% improvement over the direct solver, with generally larger improvements for greater numbers of walls. This improvement was computed as

$$\text{percentage improvement} = 100 \left(\frac{a - b}{a} \right), \quad (22)$$

where, here, a and b represent the mean objective values obtained from the RBFOpt-D and RBFOpt-PL solvers. The same metric is also used throughout Tables 2, 3, and 4.

A similar comparison is made between DE-D and DE-PL in Table 2. Again, the pathline-based solver (DE-PL) outperformed its direct counterpart (DE-D) in nearly all metrics, providing an overall mean improvement of 59%. The pathline-based solver also displayed mostly monotonic decreases in the objective as the number of walls increased, while the objectives associated with the direct solver generally *increased* as the number of walls increased. However, note that for small numbers of walls (i.e., one and two), the direct DE solver outperformed its pathline-based counterpart. This could be a conse-

435 quence of the more complicated objective penalty in Constraint (21b) when \mathcal{P} is restricted.
436 For example, Deb (2000) describes various means by which penalty-based genetic algo-
437 rithms can result in nonoptimal solutions. Nonetheless, overall, the direct penalization
438 method considered herein works well.

439 It is important to note the differences between the RBFOpt-based and DE-based
440 solvers benchmarked in Tables 1 and 2, respectively. In general, DE-PL greatly outper-
441 formed both RBFOpt-based solvers; for example, DE-PL provided a 47% mean improve-
442 ment over RBFOpt-PL. These differences could be for multiple reasons. For example,
443 there are many more hyperparameters associated with RBFOpt than DE; more careful
444 tuning may have increased RBFOpt's convergence. Furthermore, RBFOpt's `sampling`
445 search strategy was used to show the efficacy of the pathline-based approach when ap-
446 plied to other (non-evolutionary) search techniques; the solver software may have per-
447 formed more favorably using some other strategy.

448 Figure 4 displays the best obtained wall configuration for each possible number of
449 walls using the DE-PL solver. Structure placement appears highly nonincremental as the
450 number of walls increases, especially for smaller numbers of walls. Also, when optimiz-
451 ing for a number of walls greater than eight, solutions generally deteriorated, indicat-
452 ing the search space becomes prohibitively large. Interestingly, the size of the restricted
453 set $\tilde{\mathcal{P}}$ did not increase substantially as the configuration size grew. Finally, in Figure 5,
454 the best obtained solution for ten walls using DE-D is displayed; this underscores the
455 difficulty of such a problem when applying a conventional algorithm.

456 *4.4.2 Sequential algorithm results*

457 To counteract the degradation of solutions for larger configurations, the sequen-
458 tial approach presented in Section 3.2 was benchmarked in a similar setting. In Table
459 3, performance of the direct sequential DE solver (DE-D-S) is compared against DE-PL.
460 Interestingly, DE-D-S performed much better than DE-PL for configurations contain-
461 ing many walls, providing improvements as large as 84%. This result indicates the dif-
462 ficulty in optimizing configurations of multiple structural mitigation measures simulta-
463 neously, which may lead to a worse objective when running the previous algorithms with
464 more measures. Note, however, that the sequential approach generally did not provide
465 improvements over DE-PL for configurations consisting of three, four, and five walls. These

466 results indicate that sequential optimization is most beneficial when the number of struc-
467 tural measures becomes larger (e.g., greater than five).

468 Finally, a comparison between DE-D-S and the sequential DE-PL solver (DE-PL-
469 S) is made in Table 4. On average, DE-PL-S provided a 24% improvement over its di-
470 rect counterpart. The sequential DE-PL solver was also capable of finding a solution which
471 completely mitigated the flood using a smaller structural budget. That is, the direct se-
472 quential solver found a totally mitigating solution at $m = 9$, but DE-PL-S accomplished
473 this for $m = 8$. Interestingly, however, for $m = 10$, DE-D-S found a totally mitigat-
474 ing solution, whereas DE-PL-S only found a *nearly* mitigating solution. This again may
475 be a consequence of the relatively small number of experiments performed. Overall, ex-
476 cept for small m (i.e., $m = 1$), the pathline-based sequential approach appears highly
477 superior to the direct sequential approach. This result indicates that DE-PL-S serves as
478 a good general purpose OFMP solver.

479 Figure 6 displays the ten incremental configurations obtained via DE-PL-S for $m =$
480 10 and the random seed that gave the minimum corresponding objective in Table 4. The
481 ultimate solution for $m = 10$ shows remarkable similarity to the solution obtained via
482 DE-PL for $m = 8$, as shown in Figure 4. That is, both solutions appear to exploit the
483 critical depth boundary condition to divert water outside of the domain’s uppermost bound-
484 ary. However, the sequential solution appears to place a larger number of walls in more
485 intuitive locations. Similarly, as displayed by the solution for $m = 10$ shown in Figure
486 7, DE-D-S also produced a configuration which diverted flow out of the domain’s upper-
487 most boundary, although one wall was placed extraordinarily near this boundary. Such
488 solutions may not be possible when using the pathline approach, as pathlines typically
489 do not reside near domain boundaries.

490 **4.4.3 Summary of algorithm comparisons**

491 Tables 1 through 4 compare the performance of solvers against one another. Within
492 these tables, the best objectives over *all* seeds and solvers are denoted in bold, while the
493 best *mean* objectives are underlined. It is first apparent that for $m \in \{1, 2\}$, minima
494 were obtained through use of DE-D. Good mean objectives were also obtained using this
495 solver. This result indicates that direct local search algorithms are capable of perform-

496 ing well on OFMPs that contain a small number of structural measures. It also implies
497 that more careful tuning of these algorithms may hold great promise.

498 For $m = 3$, DE-PL performed most favorably, providing the best overall and best
499 mean objectives. This implies for a moderate number of structural measures, DE-PL ef-
500 fectively uses pathlines to restrict the search space. Moreover, if the optimal solution is
501 nonincremental, it is capable of finding solutions that sequential approaches cannot. How-
502 ever, for $m > 3$, DE-PL-S performs most favorably, indicating a combination of pathline-
503 based and sequential approaches are needed to solve challenging problems.

504 *4.4.4 Proof of concept for soft structural mitigation measures*

505 Sections 4.3 through 4.4.3 focus on OFMPs designed to configure the placement
506 of *hard* structural mitigation measures (i.e., $\bar{b}_i > 0$ and $\bar{n}_i = 0$). However, it is im-
507 portant to emphasize that the problem formulations and techniques described through-
508 out Sections 2, 3, and 4.1 are not limited to such measures. To exemplify this, a proof
509 of concept employing only soft structural measures is assessed. In particular, an OFMP
510 taking the form of Equations (21a) through (21g) is proposed that optimizes the con-
511 figuration of m revegetation projects (i.e., $\bar{n}_i > 0$ and $\bar{b}_i = 0$).

512 Using the ICOLD 2013 scenario, the above problem was constructed for a num-
513 ber of revegetation projects ranging from one to ten. Each revegetation project was as-
514 sumed to have a radius of 250 meters and increased the Manning's roughness coefficient
515 in the project region from 0.035 to 0.123. An experimental setting equivalent to that de-
516 scribed in Section 4.2 was used. However, in these experiments, only the DE and DE-
517 PL solvers were compared. Furthermore, only a single random seed was used.

518 In Figure 8, for each experiment, the objective behavior is plotted against the num-
519 ber of PDE evaluations required to reach that objective. The DE-PL solver was gener-
520 ally able to improve upon solutions more rapidly, especially for configurations involving
521 larger numbers of revegetation projects. These results mimic the behaviors of Figure 2,
522 Table 1, and Table 2. That is, for smaller numbers of projects, the direct algorithm is
523 sufficient, but for larger numbers of projects, the pathline-based algorithm is needed to
524 obtain meaningful solutions.

525 Finally, in Figure 9, the configurations using DE-PL are displayed pictorially for
526 all pairs of scenarios and numbers of projects. The results are highly intuitive upon greater
527 inspection. First, many of the projects appear to be placed in locations that interdict
528 the initial flood wave. More interestingly, many are located along the primary channels
529 of the scenario domain, where larger velocities would occur. This makes sense, as the bed
530 shear stress source terms are proportional to the square of velocity; measures that in-
531 crease roughness are thus highly beneficial in these regions.

532 5 Conclusion

533 This study addressed the difficult problem of designing structural flood risk man-
534 agement strategies for use within the risk assessment process. To this end, an optimization-
535 based decision support approach was proposed for designing mitigation strategies. A num-
536 ber of numerical methodologies were developed that generally function through modi-
537 fying the bed slope and bed shear stress source terms of the 2D shallow water equations.
538 However, the methodologies are sufficiently general to modify other source terms (e.g.,
539 adjustment of soil properties that affect \mathbf{S}_R via infiltration) or even supplant the shal-
540 low water equations with a different physical model.

541 To formalize the mitigation task, the Optimal Flood Mitigation Problem (OFMP)
542 was introduced. To solve practical problems of this type, a time-limited search-based op-
543 timization algorithm was developed. Within this algorithm, three approaches to gener-
544 ate solutions were explored: a direct approach using only derivative-free optimization,
545 an augmented approach using pathlines to restrict the search space, and a sequential op-
546 timization approach. The latter two were largely successful, depending on the number
547 of mitigation measures defined in the OFMP. Overall, the non-sequential and sequen-
548 tial pathline-based differential evolution approaches provided average improvements of
549 59% and 65% over their direct counterpart, respectively. Results illustrate the first mean-
550 ingful solutions to large-scale optimization problems of this type.

551 Future work should seek to increase and prove the applicability of the approach to
552 realistic flood scenarios. First, it should seek to generalize the approach by benchmark-
553 ing performance on a greater number of real-world flood scenarios. Second, it should ad-
554 dress the inherent uncertainty in flood scenario parameterizations (e.g., topographic el-
555 evation, dam breach parameterization, bed friction). To this end, a stochastic optimiza-

tion approach should be developed to ensure solutions are distributionally robust from a planning perspective. Third, a human behavioral study should be conducted to compare the utility of the optimization approach presented herein with the typically manual process used in simulation-based mitigation design. Fourth, algorithmic enhancements should be made to increase the realism of mitigation designs. For example, flood walls used in the numerical experiments were overtoppable. This may not be realistic from a flood risk management perspective. Such realism can be embedded within the optimization problem in the form of additional penalties (e.g., when walls are overtopped, a penalty is introduced) or additional constraints. Finally, the approach should be extended to solve OFMPs for scenarios that require modeling at finer spatial resolutions. To accomplish this, a multi-resolution approach should be developed, where the spatial resolution of a flood scenario is iteratively refined as optimization progresses. This work would be valuable for realistic scenarios, where fine resolution details are sometimes necessary to accurately predict flooding behavior.

A **ComputePathline**(\mathbf{U}, x_0, y_0)

In Algorithm 3, Line 2, the pathline and current pathline segment lengths, L and ℓ , are initialized to zero, and the pathline-describing point set \mathcal{L} is initialized. In Line 3, the integration loop is defined. Integration halts once the total pathline length is greater than some predefined threshold, L_{\max} , or the time falls outside the interval of interest, $[t_0, t_{\text{wet}}]$, where t_{wet} is calculated as per Equation (17). In Line 4, the discrete solution indices are obtained. Here, $\text{GETINDEX}(x, y)$ is a function that maps the spatial coordinates (x, y) to the corresponding spatial index on the rectangular solution grid G , (i, j) . Similarly, the time index k is obtained by computing the index of the ordered timestamp set \mathcal{T} corresponding to the least absolute difference with the current integration time t . In Lines 5 through 7, the loop is terminated if the current speed or depth is smaller than some arbitrarily small constant ϵ_m .

In Line 8, the time step is computed to (approximately) ensure the integrated distance will not be greater than one third the length of a grid cell. In Line 9, the first step of second-order Runge-Kutta integration is performed. In Lines 10 through 12, the loop is terminated if the point suggested by the previous integration step falls outside the flood scenario's spatial domain, denoted as $D(\mathbf{U})$. In Line 13, the discrete indices of the proposed solution are obtained. In Lines 14 through 16, the loop is terminated if the depth

Algorithm 3 COMPUTEPATHLINE: Approximates a pathline emanating to some point.

```

1: function COMPUTEPATHLINE( $\mathbf{U}, x_0, y_0$ )
2:    $L \leftarrow 0, \ell \leftarrow 0, x \leftarrow x_0, y \leftarrow y_0, t \leftarrow t_{\text{wet}}(x_0, y_0), \mathcal{L} \leftarrow \{(x_0, y_0)\}$ 
3:   while  $L < L_{\text{max}}$  and  $t \in [t_0, t_{\text{wet}}(x_0, y_0)]$  do
4:      $(i, j) \leftarrow \text{GETINDEX}(x, y), k \leftarrow \text{argmin} \{\tau \in \mathcal{T}(\mathbf{U}) : |t - \tau|\}$ 
5:     if  $\sqrt{u_{ijk}^2 + v_{ijk}^2} \leq \epsilon_m$  or  $h_{ijk} \leq \epsilon_m$  then
6:       break
7:     end if
8:      $\Delta t \leftarrow -\frac{1}{3} \min \left( \frac{\Delta x}{|u_{ijk}|}, \frac{\Delta y}{|v_{ijk}|} \right)$ 
9:      $x_* \leftarrow x + u_{ijk} \Delta t, y_* \leftarrow y + v_{ijk} \Delta t, t_* = t + \Delta t$ 
10:    if  $(x_*, y_*) \notin D(\mathbf{U})$  then
11:      break
12:    end if
13:     $(i_*, j_*) \leftarrow \text{GETINDEX}(x_*, y_*), k_* \leftarrow \text{argmin} \{\tau \in \mathcal{T}(\mathbf{U}) : |t_* - \tau|\}$ 
14:    if  $h_{i_*, j_*, k_*} \leq \epsilon_m$  then
15:      break
16:    end if
17:     $x_n \leftarrow x + \frac{1}{2} \Delta t (u_{ijk} + u_{i_*, j_*, k_*}), y_n \leftarrow y + \frac{1}{2} \Delta t (u_{ijk} + u_{i_*, j_*, k_*})$ 
18:     $\Delta s \leftarrow \sqrt{(x_n - x)^2 + (y_n - y)^2}$ 
19:    if  $(x_n, y_n) \notin D(\mathbf{U})$  or  $\Delta s \leq \epsilon_m$  or  $\Delta s > 2\alpha$  then
20:      break
21:    end if
22:     $L \leftarrow L + \Delta s, \ell \leftarrow \ell + \Delta s$ 
23:     $x \leftarrow x_n, y \leftarrow y_n, t \leftarrow t_*$ 
24:    if  $\ell \geq \frac{1}{2}(\Delta x + \Delta y)$  then
25:       $\ell \leftarrow 0, \mathcal{L} \leftarrow \mathcal{L} \cup \{(x_n, y_n)\}$ 
26:    end if
27:  end while
28:  return  $\mathcal{L}$ 
29: end function

```

588

at the proposed index is too small. In Line 17, the second Runge-Kutta integration step

589

is performed. In Lines 19 through 21, the loop is terminated if the integrated point falls

590 outside $D(\mathbf{U})$, if the change was small, or if the change was very large (where α is some
 591 predefined fixed distance). In Line 22, the total pathline and temporary segment lengths
 592 are updated using the most recent integration distance. In Line 23, the relevant variables
 593 are integrated. In Lines 24 through 26, the temporary segment length is reset to zero
 594 and the pathline approximation is updated if the segment length is greater than or equal
 595 to the mean grid cell spacing.

596 B AlphaShape(Q, α)

597 In Algorithm 4, DELAUNAY(Q, α) is a function that computes the *Delaunay tri-*
 598 *angulation* for a set Q of discrete points. A Delaunay triangulation is a set of triangles
 599 such that no point in Q is contained within the circumscribed circle of any triangle. A
 600 number of algorithms exist to compute this triangulation; herein, that of Barber, Dobkin,
 and Huhdanpaa (1996) is used.

Algorithm 4 ALPHASHAPE: Computes an alpha shape from a discrete set of points Q .

```

1: function ALPHASHAPE( $Q, \alpha$ )
2:    $\mathcal{D} \leftarrow \text{DELAUNAY}(Q)$ ,  $\mathcal{B} \leftarrow \emptyset$ 
3:   for  $\Delta \in \mathcal{D}$  do
4:      $(a, b, c) \leftarrow \text{GETVERTICES}(\Delta)$ 
5:      $d_a \leftarrow \|a - b\|$ ,  $d_b \leftarrow \|b - c\|$ ,  $d_c \leftarrow \|c - a\|$ 
6:      $s \leftarrow \frac{1}{2}(d_a + d_b + d_c)$ 
7:      $A \leftarrow \sqrt{s(s - d_a)(s - d_b)(s - d_c)}$ 
8:     if  $A = 0$  then
9:       continue
10:    else if  $\frac{d_a d_b d_c}{4A} < \alpha$  then
11:       $\mathcal{B} \leftarrow \mathcal{B} \cup \Delta$ 
12:    end if
13:  end for
14:  return  $\mathcal{B}$ 
15: end function

```

601

602 In Line 2 of Algorithm 4, the set of Delaunay triangles \mathcal{D} is computed for the point
 603 set Q , and the set \mathcal{B} comprising the triangular regions of the alpha shape is initialized

604 as the empty set. In Line 4, the function `GETVERTICES(Δ)` is used to obtain the ver-
 605 tex positions of the triangle Δ . In Line 5, the Euclidean edge distances are computed
 606 for the triangle Δ . In Line 6, the semiperimeter s of the triangle Δ is computed. In Line
 607 7, the area of the triangle Δ is computed via Heron's formula. In Line 11, if the circum-
 608 scribed radius of the triangle is less than the constant α , the triangle is unioned with the
 609 set \mathcal{B} describing the alpha shape. In this paper, α is always taken to be $5(\Delta x + \Delta y)/2$,
 610 where Δx and Δy are the grid cell spacings used to discretize the spatial domain in the
 611 x - and y - directions, respectively.

612 Acknowledgments

613 All primary input and output data for the experiments described in this study are
 614 publicly available at [http://nuflood.com/documents/resources/tasseff-2018a.tar](http://nuflood.com/documents/resources/tasseff-2018a.tar.gz)
 615 [.gz](http://nuflood.com/documents/resources/tasseff-2018a.tar.gz). This material is based upon work supported by the National Science Foundation
 616 Graduate Research Fellowship under Grant No. DGE-1256260 and under the auspices
 617 of the National Nuclear Security Administration of the U.S. Department of Energy at
 618 Los Alamos National Laboratory under Contract No. DE-AC52-06NA25396.

619 References

- 620 Barber, C. B., Dobkin, D. P., & Huhdanpaa, H. (1996). The quickhull algorithm for
 621 convex hulls. *ACM Transactions on Mathematical Software (TOMS)*, *22*(4),
 622 469–483.
- 623 Brekelmans, R., den Hertog, D., Roos, K., & Eijgenraam, C. (2012, December).
 624 Safe dike heights at minimal costs: The nonhomogeneous case. *Operations Re-*
 625 *search*, *60*(6), 1342–1355. Retrieved from [http://pubsonline.informs.org/](http://pubsonline.informs.org/doi/abs/10.1287/opre.1110.1028)
 626 [doi/abs/10.1287/opre.1110.1028](http://pubsonline.informs.org/doi/abs/10.1287/opre.1110.1028) doi: 10.1287/opre.1110.1028
- 627 Brodtkorb, A. R., Sætra, M. L., & Altinakar, M. (2012). Efficient shallow water sim-
 628 ulations on GPUs: Implementation, visualization, verification, and validation.
 629 *Computers & Fluids*, *55*, 1–12.
- 630 Che, D., & Mays, L. W. (2015, June). Development of an optimization/simulation
 631 model for real-time flood-control operation of river-reservoirs systems.
 632 *Water Resources Management*, *29*(11), 3987–4005. Retrieved from
 633 <http://link.springer.com/10.1007/s11269-015-1041-8> doi: 10.1007/
 634 [s11269-015-1041-8](http://link.springer.com/10.1007/s11269-015-1041-8)

- 635 Chertock, A., Cui, S., Kurganov, A., & Wu, T. (2015). Well-balanced positivity
636 preserving central-upwind scheme for the shallow water system with friction
637 terms. *International Journal for Numerical Methods in Fluids*, 78(6), 355–
638 383. Retrieved from <http://dx.doi.org/10.1002/flid.4023> (fld.4023) doi:
639 10.1002/flid.4023
- 640 Colombo, R. M., Guerra, G., Herty, M., & Schleper, V. (2009, January). Optimal
641 control in networks of pipes and canals. *SIAM Journal on Control and Opti-*
642 *mization*, 48(3), 2032–2050. Retrieved from [http://epubs.siam.org/doi/](http://epubs.siam.org/doi/abs/10.1137/080716372)
643 [abs/10.1137/080716372](http://epubs.siam.org/doi/abs/10.1137/080716372) doi: 10.1137/080716372
- 644 Costa, A., & Nannicini, G. (2014). RBFOpt: an open-source library for black-box
645 optimization with costly function evaluations. *Optimization Online*, 4538.
- 646 Deb, K. (2000). An efficient constraint handling method for genetic algorithms.
647 *Computer Methods in Applied Mechanics and Engineering*, 186(2), 311 - 338.
648 Retrieved from [http://www.sciencedirect.com/science/article/pii/](http://www.sciencedirect.com/science/article/pii/S0045782599003898)
649 [S0045782599003898](http://www.sciencedirect.com/science/article/pii/S0045782599003898) doi: [https://doi.org/10.1016/S0045-7825\(99\)00389-8](https://doi.org/10.1016/S0045-7825(99)00389-8)
- 650 Edelsbrunner, H., Kirkpatrick, D., & Seidel, R. (1983). On the shape of a set of
651 points in the plane. *IEEE Transactions on Information Theory*, 29(4), 551–
652 559.
- 653 Fischer, K. (2000). *Introduction to alpha shapes*. [https://graphics.stanford.edu/](https://graphics.stanford.edu/courses/cs268-11-spring/handouts/AlphaShapes/as_fisher.pdf)
654 [courses/cs268-11-spring/handouts/AlphaShapes/as_fisher.pdf](https://graphics.stanford.edu/courses/cs268-11-spring/handouts/AlphaShapes/as_fisher.pdf). (Ac-
655 cessed: 2017-09-19)
- 656 Judi, D., Tasseff, B., Bent, R., & Pan, F. (2014). *LA-UR 14-21247: Topography-*
657 *based flood planning and optimization capability development report* (Tech.
658 Rep.). Los Alamos National Laboratory.
- 659 Judi, D. R., Pasqualini, D., & Arnold, J. D. (2014). *Computational challenges in*
660 *consequence estimation for risk assessment-numerical modelling, uncertainty*
661 *quantification, and communication of results* (Tech. Rep.). Los Alamos Na-
662 tional Laboratory (LANL).
- 663 Kurganov, A., & Petrova, G. (2007). A second-order well-balanced positivity pre-
664 serving central-upwind scheme for the Saint-Venant system. *Communications*
665 *in Mathematical Sciences*, 5(1), 133–160.
- 666 Sayers, P., Yuanyuan, L., Galloway, G., Penning-Rowsell, E., Fuxin, S., Kang, W.,
667 ... Le Quesne, T. (2013). *Flood risk management: A strategic approach*. Asian

- 668 Development Bank, GIWP, UNESCO, and WWF-UK.
- 669 Storn, R., & Price, K. (1997). Differential evolution – a simple and efficient heuristic
670 for global optimization over continuous spaces. *Journal of Global Optimization*,
671 11(4), 341–359.
- 672 Tasseff, B. (2016). *Nuflood, Version 1.x* (Tech. Rep.). Los Alamos National Labora-
673 tory (LANL), Los Alamos, NM (United States).
- 674 Tasseff, B., Bent, R., & Van Hentenryck, P. (2016). Optimal flood mitigation over
675 flood propagation approximations. In *International Conference on AI and*
676 *OR Techniques in Constraint Programming for Combinatorial Optimization*
677 *Problems* (pp. 358–373).
- 678 Telea, A. C. (2014). *Data visualization: principles and practice*. CRC Press.

m	RBFOpt-D				RBFOpt-PL				Mean
	Mean	Min	Max	SD	Mean	Min	Max	SD	Improvement
1	165.93	159.63	170.25	3.36	162.81	159.63	167.59	2.61	1.88%
2	147.96	105.34	166.60	20.14	111.02	95.98	130.88	10.74	24.96%
3	144.93	111.87	164.10	15.44	89.22	77.56	93.62	5.40	38.44%
4	128.52	105.81	159.12	14.21	81.33	51.63	97.83	13.47	36.72%
5	135.94	128.25	144.42	5.03	62.38	26.40	80.40	15.67	54.11%
6	122.24	98.38	140.19	14.22	59.13	41.40	71.25	9.07	51.63%
7	119.14	81.14	145.80	18.65	51.11	29.13	66.20	13.08	57.10%
8	102.08	78.65	122.69	16.22	43.28	27.82	57.35	9.40	57.60%
9	107.40	81.93	127.53	15.52	42.73	19.00	53.26	11.19	60.21%
10	104.90	77.17	124.13	16.75	34.72	21.75	42.74	7.60	66.90%

679 **Table 1.** Table comparing objectives using the (direct) RBFOpt-D and (pathline-based)
680 RBFOpt-PL solvers over ten random seeds, with the number of walls (m) ranging from one to
681 ten, as discussed in Section 4.4. Values are scaled by a factor of 10^{-4} .

m	DE-D				DE-PL				Mean
	Mean	Min	Max	SD	Mean	Min	Max	SD	Improvement
1	<u>162.18</u>	158.59	167.59	3.85	163.86	159.63	170.07	4.52	-1.04%
2	99.49	84.87	104.24	6.29	102.61	94.24	105.39	3.19	-3.13%
3	66.78	39.56	119.20	27.76	<u>50.75</u>	33.36	65.93	14.80	24.01%
4	101.06	79.57	134.61	20.57	31.84	17.51	56.87	13.20	68.49%
5	115.43	100.56	145.39	16.04	22.74	12.82	36.39	8.04	80.30%
6	124.15	101.22	145.75	15.85	24.79	7.24	60.66	14.87	80.03%
7	129.17	110.94	153.14	12.52	18.14	5.59	26.77	6.64	85.96%
8	125.51	96.68	144.92	16.47	14.02	4.03	19.74	5.59	88.83%
9	129.23	99.39	146.58	14.02	17.83	8.56	22.46	4.85	86.20%
10	119.09	86.16	140.87	17.91	19.68	10.43	30.38	5.61	83.47%

682 **Table 2.** Table comparing objective values obtained using the (direct) DE-D and (pathline-
683 based) DE-PL solvers over ten random seeds, with the number of walls (m) ranging from one to
684 ten. Values are scaled by a factor of 10^{-4} . Best objectives over all seeds and solvers in Tables 1
685 through 4 are denoted in bold, while best *mean* objectives are underlined.

m	DE-PL				DE-D-S				Mean
	Mean	Min	Max	SD	Mean	Min	Max	SD	Improvement
1	163.86	159.63	170.07	4.52	<u>162.18</u>	158.59	167.59	3.85	1.02%
2	102.61	94.24	105.39	3.19	102.38	100.97	103.68	0.87	0.22%
3	<u>50.75</u>	33.36	65.93	14.80	64.98	48.97	81.93	14.71	-28.06%
4	31.84	17.51	56.87	13.20	41.04	26.07	58.60	14.88	-28.89%
5	22.74	12.82	36.39	8.04	23.22	17.45	34.87	6.18	-2.11%
6	24.79	7.24	60.66	14.87	14.94	11.56	18.39	2.26	39.76%
7	18.14	5.59	26.77	6.64	11.14	4.10	14.53	2.87	38.60%
8	14.02	4.03	19.74	5.59	9.42	6.02	16.64	3.30	32.81%
9	17.83	8.56	22.46	4.85	4.72	0.00	9.91	3.74	73.52%
10	19.68	10.43	30.38	5.61	3.07	0.00	9.29	3.10	84.38%

686 **Table 3.** Table comparing objective values obtained using the (pathline-based) DE-PL and
687 (direct sequential) DE-D-S solvers over ten random seeds, with the number of walls (m) ranging
688 from one to ten. Values are scaled by a factor of 10^{-4} . Best objectives over all seeds and solvers
689 in Tables 1 through 4 are denoted in bold, while best *mean* objectives are underlined.

m	DE-D-S				DE-PL-S				Mean
	Mean	Min	Max	SD	Mean	Min	Max	SD	Improvement
1	<u>162.18</u>	158.59	167.59	3.85	163.61	159.63	167.59	4.19	-0.88%
2	102.38	100.97	103.68	0.87	<u>98.25</u>	86.78	105.84	7.45	4.04%
3	64.98	48.97	81.93	14.71	56.74	35.73	86.12	13.92	12.69%
4	41.04	26.07	58.60	14.88	<u>27.18</u>	14.55	56.37	11.81	33.77%
5	23.22	17.45	34.87	6.18	<u>16.32</u>	8.38	25.35	5.25	29.73%
6	14.94	11.56	18.39	2.26	<u>10.63</u>	3.92	16.96	5.29	28.82%
7	11.14	4.10	14.53	2.87	<u>7.02</u>	0.13	15.00	5.08	36.97%
8	9.42	6.02	16.64	3.30	<u>4.53</u>	0.00	9.68	3.81	51.90%
9	4.72	0.00	9.91	3.74	<u>3.36</u>	0.00	7.86	3.43	28.83%
10	3.07	0.00	9.29	3.10	<u>2.59</u>	0.00	6.30	2.60	15.76%

690 **Table 4.** Table comparing objectives obtained using the (direct sequential) DE-D-S and
691 (pathline-based sequential) DE-PL-S solvers over ten random seeds, with the number of walls
692 (m) ranging from one to ten. Values are scaled by a factor of 10^{-4} . Best objectives over all seeds
693 and solvers in Tables 1 through 4 are denoted in bold, while best *mean* objectives are underlined.

694 **Figure 1.** Pictorial descriptions of six simple OFMP scenarios, ordered numerically (e.g., one
695 in the upper left). Black represents nonzero topographic elevation (of height one meter); blue
696 represents nonzero initial water depth (of height one meter); and red represents assets.

697 **Figure 2.** Comparison of objective value versus number of PDE evaluations for Scenarios 1
698 through 6, respectively, using DE-D and DE-PL for configurations of one through five walls.

699 **Figure 3.** Best obtained elevations and maximum depths for configurations of one through
700 five walls for the highly simplified flood scenarios, referenced as Scenarios 1 through 6 (ver-
701 tically). Darker blue corresponds to larger maximum depths; black corresponds to nonzero
702 portions of the initial topographic elevation field; green corresponds to elevation additions via
703 the placement of walls; and red corresponds to asset locations. The orange lines represent the
704 exteriors of the final computed restricted positional sets $\tilde{\mathcal{P}}$ in Algorithm 1.

705 **Figure 4.** Best obtained elevations and maximum depths for configurations of one through
706 ten walls for the ICOLD 2013 dam failure scenario using DE-PL. Darker blue corresponds to
707 larger maximum depths; gray corresponds to the initial topographic elevation field; green corre-
708 sponds to elevation additions via the placement of walls; and red corresponds to asset locations.
709 Orange lines represent the exteriors of the final restricted positional sets $\tilde{\mathcal{P}}$ in Algorithm 1.

710 **Figure 5.** Best solution in a setting equivalent to Figure 4 for ten walls using DE-D.

711 **Figure 6.** Best obtained elevations and maximum depths for configurations of one through
712 ten walls for the ICOLD 2013 dam failure scenario using DE-PL-S. Darker blue corresponds to
713 larger maximum depths; gray corresponds to the initial topographic elevation field; green corre-
714 sponds to elevation additions via the placement of walls; and red corresponds to asset locations.
715 Orange lines represent the exteriors of the restricted positional sets $\tilde{\mathcal{P}}$ initialized in Algorithm 1.

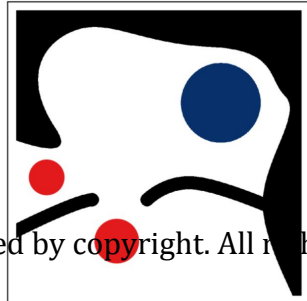
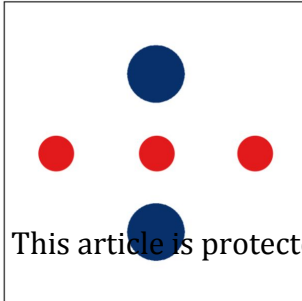
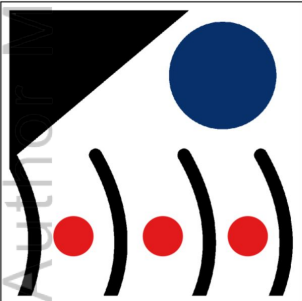
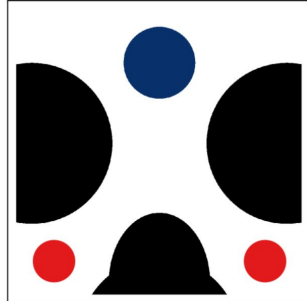
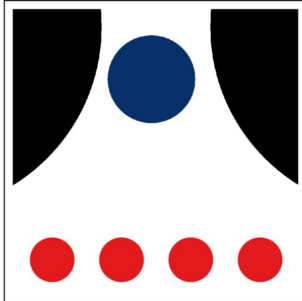
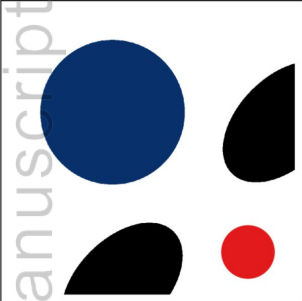
716 **Figure 7.** Best solution in a setting equivalent to Figure 6 for ten walls using DE-D-S.

717 **Figure 8.** Comparison of objective versus number of PDE evaluations for the OFMP in Sec-
718 tion 4.4.4, using DE-D and DE-PL for configurations of one through ten revegetation projects.

719 **Figure 9.** Revegetation locations and maximum depths for configurations of one through
720 ten projects for the ICOLD 2013 dam failure scenario using DE-PL. Darker blue corresponds to
721 larger maximum depths; gray corresponds to the initial topographic elevation field; green corre-
722 sponds to the placement of revegetation projects; and red corresponds to asset locations. Orange
723 lines represent the exteriors of the restricted positional sets $\tilde{\mathcal{P}}$ initialized in Algorithm 1.

Figure 1.

Author Manuscript



This article is protected by copyright. All rights reserved.

Figure 2.

Author Manuscript

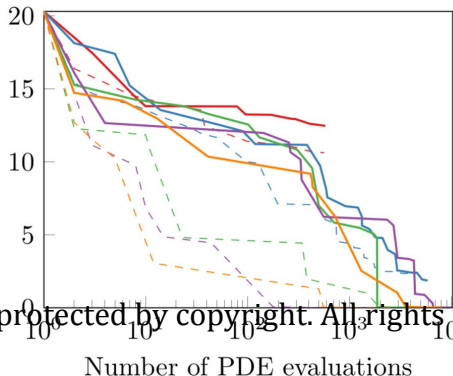
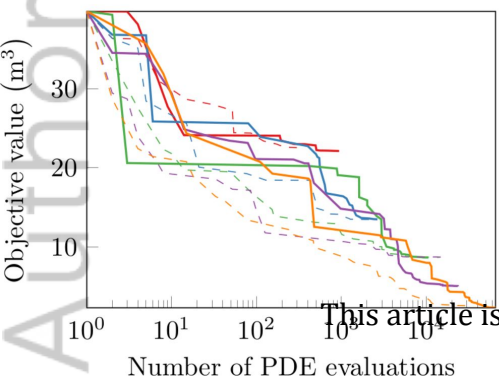
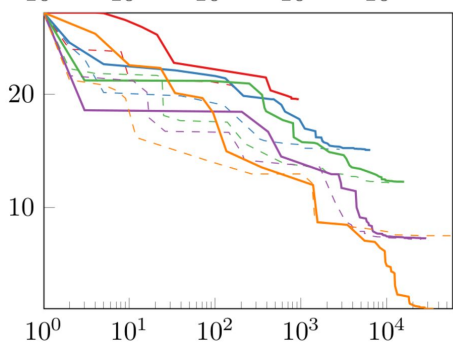
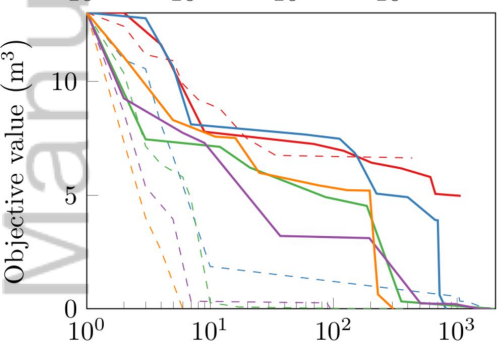
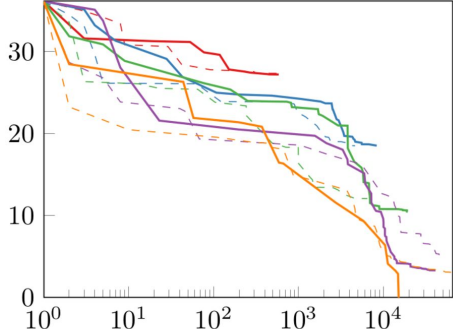
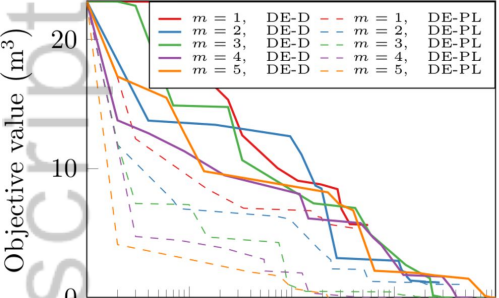


Figure 3.

Author Manuscript

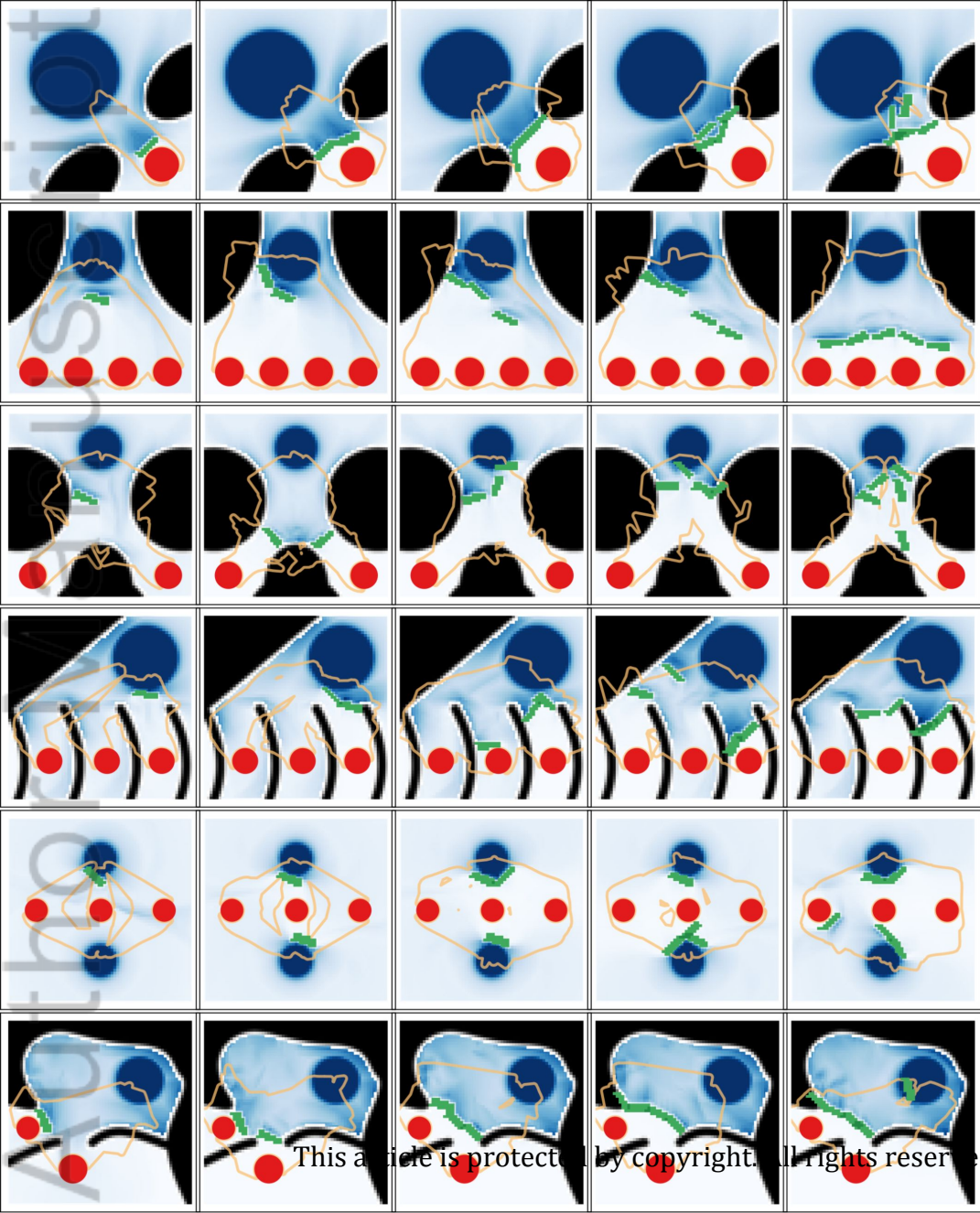


Figure 4.

Author Manuscript

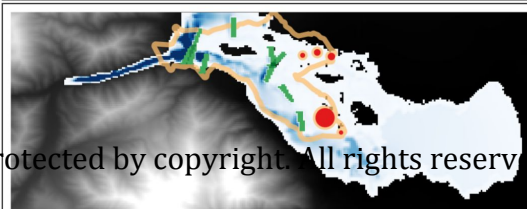
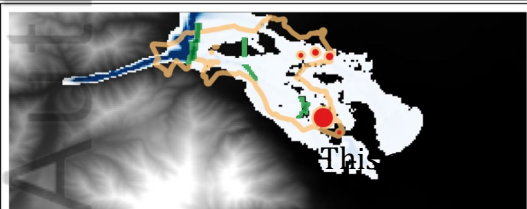
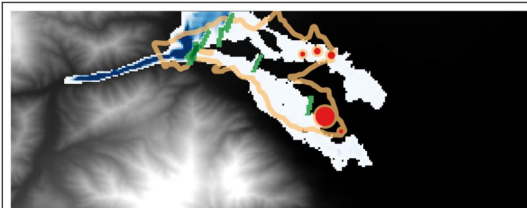
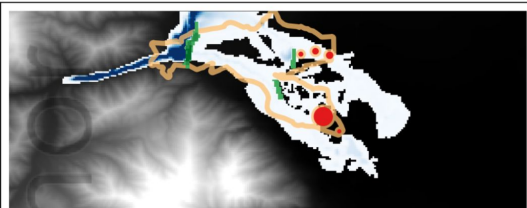
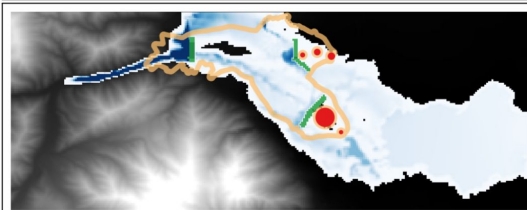
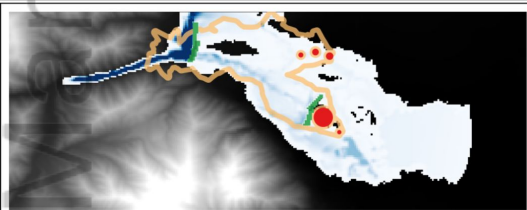
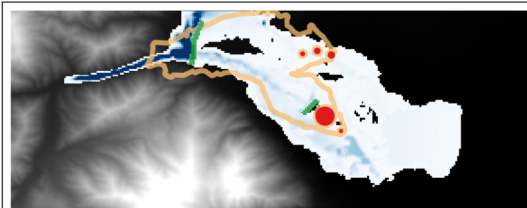
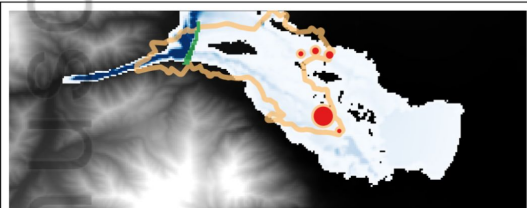
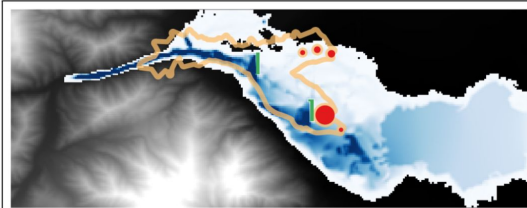
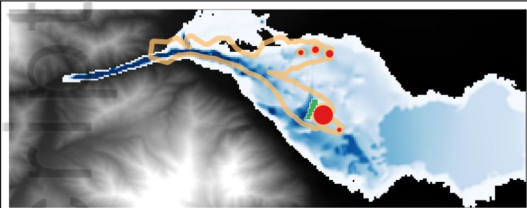


Figure 5.

Author Manuscript

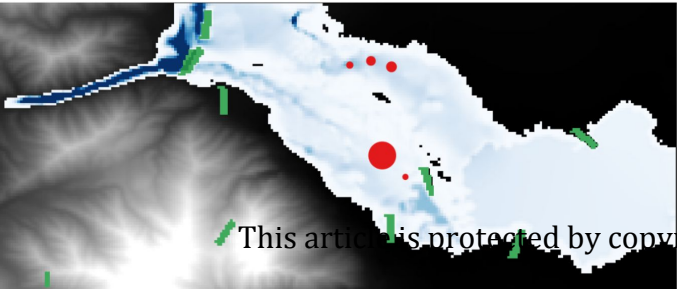
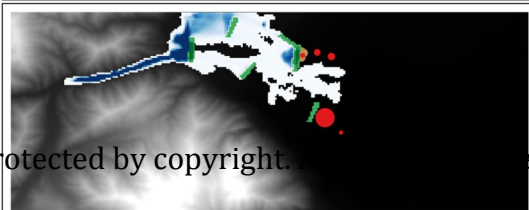
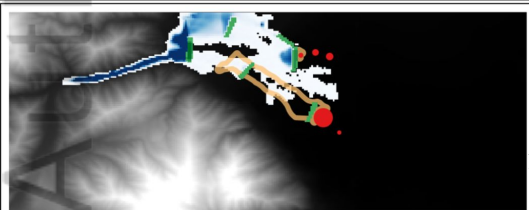
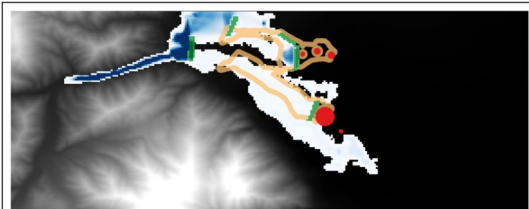
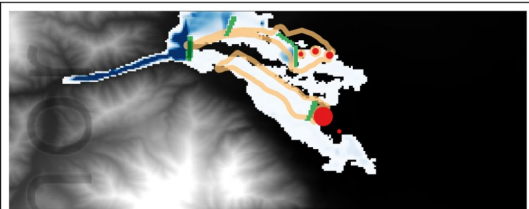
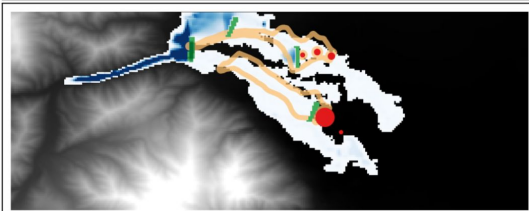
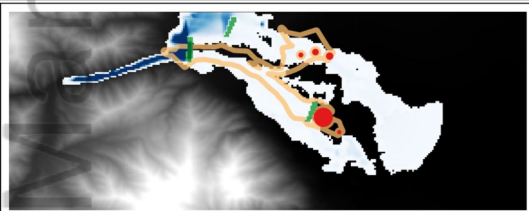
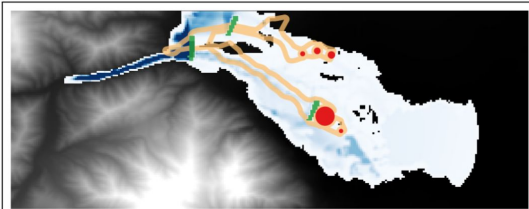
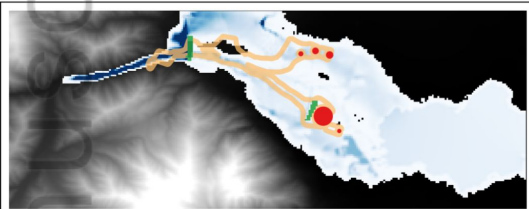
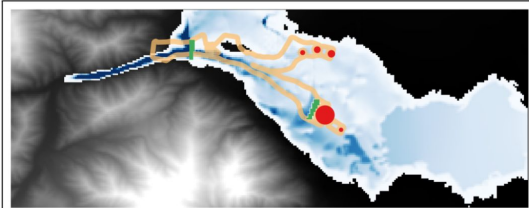
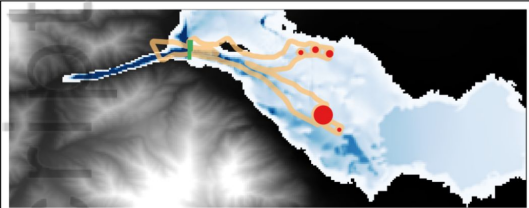


Figure 6.

Author Manuscript



protected by copyright.

Figure 7.

Author Manuscript



This article

Figure 8.

Author Manuscript

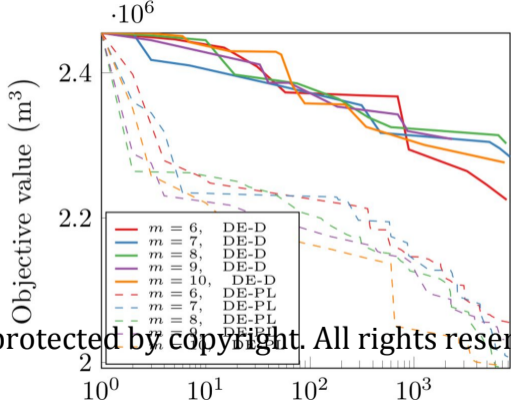
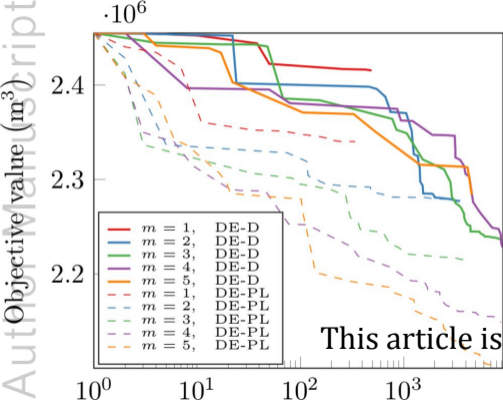
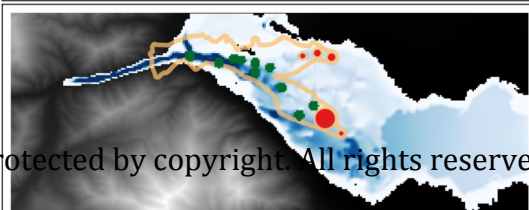
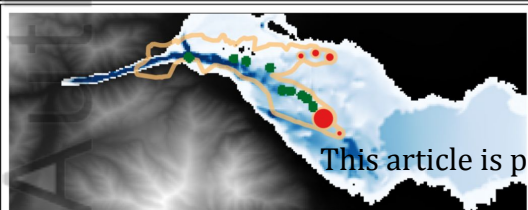
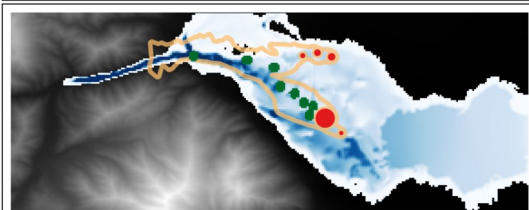
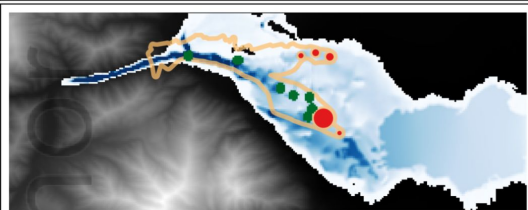
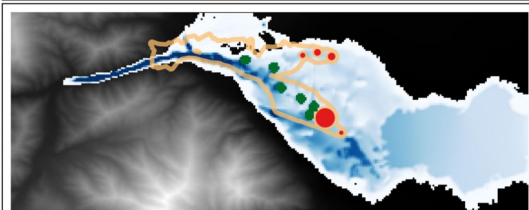
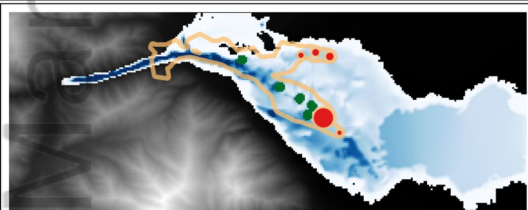
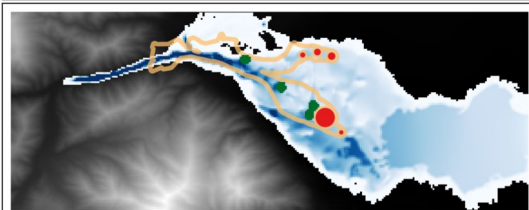
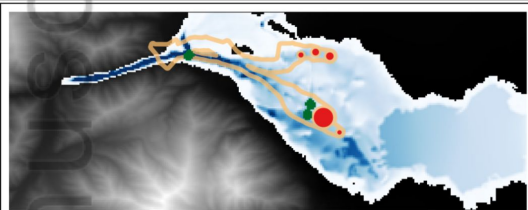
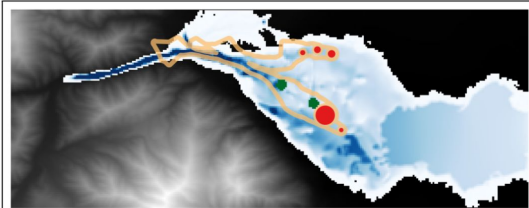
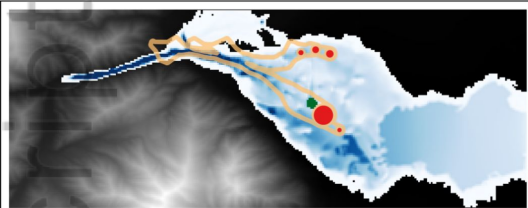


Figure 9.

Author Manuscript



This article is protected by copyright. All rights reserved.